CHAPTER 8

THERMOELECTRIC PROPERTIES OF CONDUCTING POLYMERS

Xavier Crispin
Department of Science and Technology
Campus Norrköping, Linköping University
S-60174 Norrköping, Sweden
xavier.crispin@liu.se

In response to the thread of environmental and ecological degradation along with projected fossil fuel depletion, the active search for efficient renewable energy conversion technologies has been attempted in various research areas including the field of thermoelectrics. Despite the availability of considerable amounts of waste and natural heat stored in warm fluids (<250°C), a lack of environmentally friendly materials with high natural abundance, low manufacturing cost, and high thermoelectric efficiency impedes the widespread use of thermoelectric generators for energy harvesting on a large scale. Organic conducting polymers constitute a class of materials that might be of interest for thermoelectric applications. In this chapter, we examine the possibility of using organic conducting polymers in thermoelectric applications. We provide the basic concepts in thermoelectrics and illustrate what is specific to conducting polymers. Finally, we mention some early attempts to create organic thermoelectric generators.

1. Introduction

The ability of a material to transport heat and electrical currents is dictated by the values of the thermal κ and electrical σ conductivities. The independent transport of electrons and phonons in a material is described by Ohm's law ($\vec{i} = \sigma\vec{E}$) and Fourier's law ($\vec{q} = -\kappa\vec{\nabla}T$), respectively. The thermoelectric phenomena arises in the simultaneous presence of both electrical and thermal currents. The Seebeck effect refers to the possibility of creating an electrostatic potential and thus an electrical current from a temperature gradient (see second term in Eq. (1)). A thermoelectric generator uses the Seebeck effect to convert a heat flow into an electron flow. The Peltier effect is related to the creation of a heat flow, against Joule heating, from an electrical current (see second term in Eq. (2)). This effect explains the basic mechanism of Peltier coolers.

$$\vec{i} = \sigma(\vec{E} - \alpha\vec{\nabla}T), \tag{1}$$

$$\vec{q} = -\kappa\vec{\nabla}T + \alpha T\vec{i}. \tag{2}$$

Here, E is the electric field, i is the electric current density, q is the heat current density, T is the temperature, α is the Seebeck coefficient.

Materials are characterized by a property called the Seebeck coefficient. Seebeck coefficients can be as small as few μV/K for metals and as large as several mV/K for electrical insulators.[1] The Seebeck coefficient α is the open circuit voltage obtained between the two ends of a material subjected to a temperature gradient.

$$\alpha = \left(\frac{dV}{dT}\right)_{I=0}. \tag{3}$$

The Seebeck coefficient of a material A (α_A), also called abusively thermopower, cannot be measured without the creation of two junctions subjected to a temperature gradient ΔT with another material B of well-known Seebeck coefficient α_B (Fig. 1).[2] The measure thermovoltage produced between the two junctions $V = \Delta T(\alpha_B - \alpha_A)$, allows determining α_A. Calibration can be realized with a superconductor B, since $\alpha_B = 0\,\text{V/K}$.

Figure 1(b) sketches a material in a temperature gradient with electrons as majority charge carriers. The cold side is negatively charged as a result of a longer mean-free-path of the hot electrons compared to the cold electrons. The electrons thermo-diffuse towards the cold side and the Seebeck voltage is negative. In order to know if electrons or holes are the majority carriers in an electrical conductor, one needs to look how the density-of-state is filled with carriers in an energy window k_BT centered at the Fermi level. Filling the density of state is governed by Fermi–Dirac statistics and given by the distribution $f(E) = 1/\exp((E - E_F)/k_BT) + 1$. Here, E_F is the Fermi level, k_B is the Boltzmann constant. Only charge carriers close to the Fermi level contribute to the thermodiffusion. The magnitude and sign of the Seebeck coefficient are related to an asymmetry of the electron distribution around the Fermi level. This asymmetry depends on the shape of the density of state N(E). A temperature difference over the metal in the x direction is represented by thermal broadening of the Fermi–Dirac distribution function. The hot electrons above as well

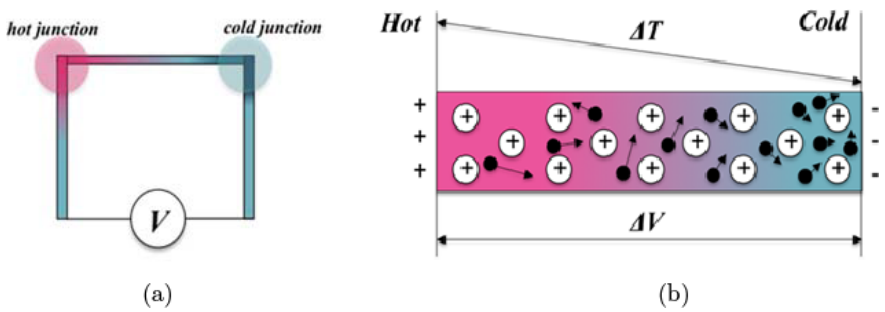

Fig. 1. (a) Seebeck effect illustration in a circuit comprising of two dissimilar materials. (b) Effect of a temperature gradient on the charge carrier diffusion in a single conductor (Olga Bubnova's courtesy).

as hot holes below the Fermi energy on the hot side thermodiffuse to the cold side, creating a current carried by electrons J_e and holes J_h. Let us assume, for the sake of simplicity, that the mobility for holes and electrons are similar. For a constant N(E) (Fig. 2(a)), the diffusion current due to the hot carriers towards lower energy region is identical for electrons and holes; as a result the Seebeck coefficient is zero. In first approximation, the magnitude of the current is proportional to the density of state. For a linearly increasing density of state vs. energy (Fig. 2(b)), the density of state for the electrons (above E_F) is larger than for holes (below E_F), as a result the electron current is larger than the hole heat current. A material with such a shape for the density of states has a net electronic current such that electrons are majority charge carriers and the cold side is negatively charged ($\alpha < 0$). On the contrary, a decreasing $N(E)$ vs. E leads to a positive Seebeck coefficient $\alpha > 0$ (Fig. 2(c)). Note the correlation between the sign of α and the slope of the density of state at the Fermi level $|dN(E)/dE|_{EF} = 0$.

2. Thermoelectric Energy Conversion

The simplest thermoelectric generator (TEG) is made of a thermoelectric material (leg) connected by two electrodes. In a thermoelectric leg of internal resistance R subject to a temperature gradient $\Delta T = T_H - T_C$, we assume that the heat propagating from the hot to the cold side can only pass through the thermoelectric legs and that the metal junction connecting the legs has a negligible electrical and thermal resistance. The thermal energy flow delivered at the hot junction is divided into three contributions (Fig. 3): (i) the rate of the heat passing through the leg $K\Delta T$ in absence of a generated electrical current (K is the thermal conductance of the thermocouple); (ii) the Joule heat $1/2I^2R$ provided to the hot side (opposite to the heat flow $K\Delta T$) originating from the generated thermoelectric current I due to the thermo-induced voltage $V = \alpha\Delta T$ (Joule heating heats the middle of the leg, so that one-half goes to each end of the leg); (iii) the rate of Peltier heat absorption $\alpha T_H I$ from the hot side due to the thermoelectric electric current going to the cold side (same direction as the heat flow $K\Delta T$). The thermal power input to the hot junction is then:

$$Q_H = \alpha T_H I - \frac{1}{2}RI^2 + K(T_H - T_C). \tag{4}$$

When the thermocouple is coupled with a load resistance R_L, the electrical power output is:

$$P = R_L I^2 \tag{5}$$

with a current:

$$I = \frac{\alpha\Delta T}{(R + R_L)}, \tag{6}$$

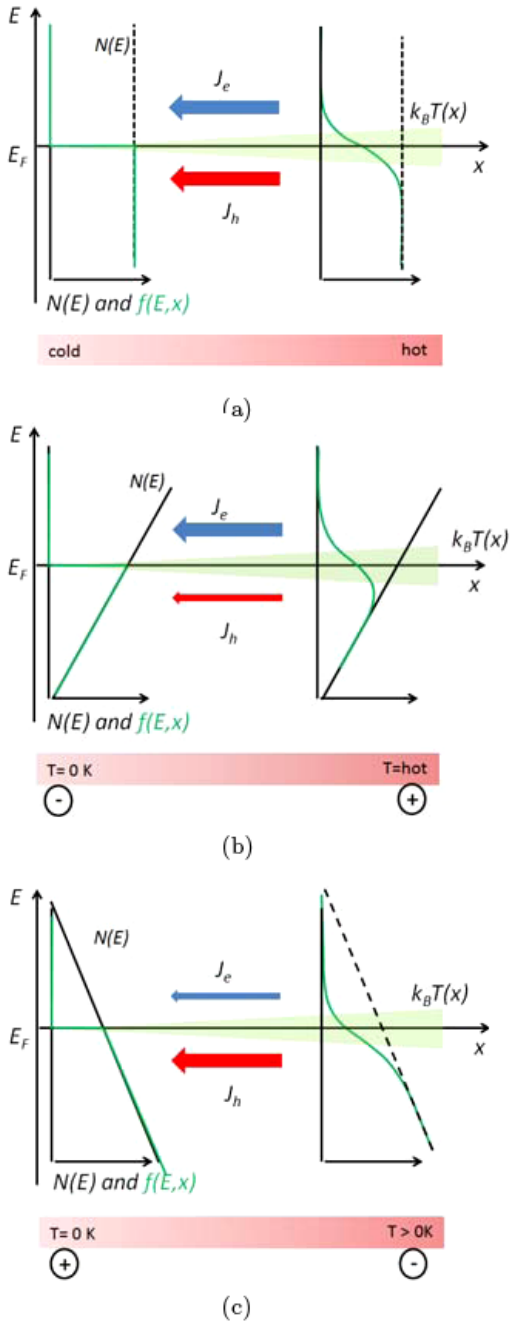

Fig. 2. (a) Case of a constant density of state N(E). The left and right sides corresponds to the cold and hot ends of the material. The Fermi distribution is plotted for the two temperatures ($T = 0\,K$ and $T > 0\,K$). (b) Case of a linearly increasing $N(E)$ with a net electron current and a negative thermopower. (c) Case of a linearly decreasing $N(E)$ that is specific of conductors with positive Seebeck coefficient.

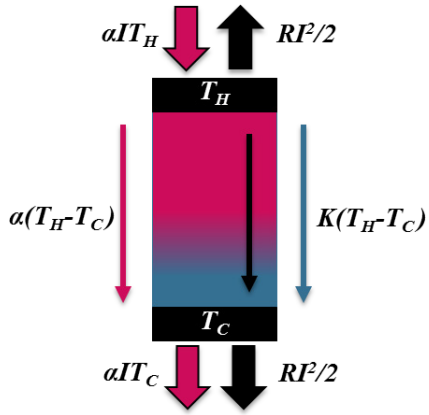

Fig. 3. Sketch of the different energy flows passing through a thermoelectric leg subjected to a temperature gradient.

and an open-circuit voltage:

$$V = \alpha \Delta T. \tag{7}$$

The efficiency η of the thermoelectric generator is the ratio between the thermal power input Q_H and the electrical power output P:

$$\eta = \frac{R_L I^2}{\left(\alpha T_H I - \frac{1}{2} I^2 R + K \Delta T\right)}. \tag{8}$$

The maximum efficiency $\eta_{\max}$ is obtained by matching the properties of the legs (length, cross section) and the load resistance to the internal resistance (further reading see e.g.,[3]). Through a simplification of the geometrical parameters, and by expressing R and K with σ and κ, $\eta_{\max}$ is given by:

$$\eta_{\max} = \frac{\Delta T}{T_H} \frac{\sqrt{1 + Z\bar{T}} - 1}{\sqrt{1 + Z\bar{T}} + \frac{T_C}{T_H}} \tag{9}$$

$$Z = \frac{\sigma \alpha^2}{\kappa}. \tag{10}$$

Z is called the thermoelectric figure of merit of a single leg regrouping the material properties (α, κ, σ); which are assumed to be constant with the temperature. ZT quantifies the ratio between the thermal energy passing through the thermoelectric element and the electrical energy produced. The evolution of the maximum efficiency vs. the temperature gradient for various Z is depicted in Fig. 4(b). A thermoelectric generator composed of a material with $ZT = 1$ is expected to reach 5% efficiency if the temperature difference between its hot and cold sides is set to 100 K.

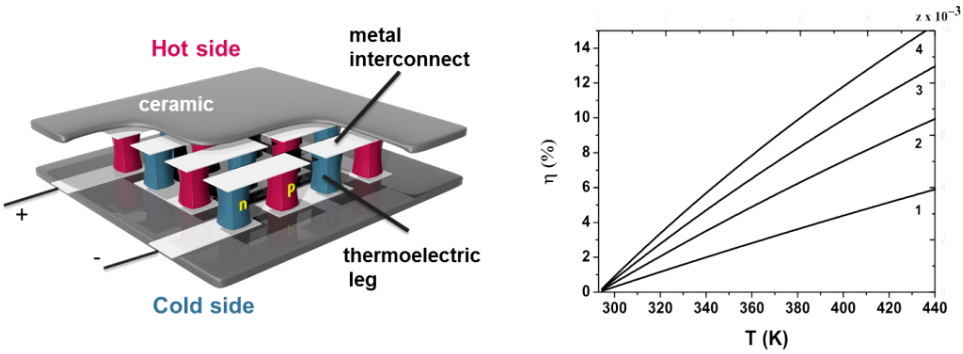

(a) (b)

Fig. 4. Sketch of a thermoelectric module composed of p-type and n-type legs (left). The conversion efficiency of the module is plotted on the right-hand side as function of the temperature for various Z values. T is the temperature of the hot side, while the cold side is maintained at 293 K.

In the regime of maximum power output, the TEG must be connected to an external load resistance equal to the internal resistance of the device $R_L = R$. The voltage output is half of the open circuit voltage $V = V_{\text{oc}}/2$ and the maximum generated power is:

$$P_{\max} = \frac{V_{\text{oc}}}{4R} = \frac{\alpha(T_H - T_C)^2}{4R}. \tag{11}$$

The conditions for maximum power output and maximum conversion efficiency at fixed geometry of the legs are not the same. Therefore, a TEG can be operated in two different modes. At constant temperature gradient, the power output increases as the legs become shorter (low internal resistance) since the unfavorable Joule heating contribution is reduced (see Eq. (4)). Now, changing the length of the leg allows setting various temperature gradients. To improve the TEG's maximum efficiency, longer legs are required, so that eventually any thermoelectric module is designed under optimal conditions dictated by a trade-off between $P_{\max}$ and $\eta_{\max}$.

For TEG to be compatible with electronics, motors or charge a battery, the thermo-induced potential must reach of the order of one volt. Because the Seebeck voltage produced by a single leg is small ($\alpha = \sim 100\,\mu V/K$), a strategy to increase the voltage is to connect thermoelectric legs electrically in series and thermally in parallel. This is called a thermoelectric module (Fig. 4); and it can either be operated as TEG or Peltier cooler. The device is sandwiched between ceramic layers to avoid short-circuiting between the metal interconnects and to ensure a good thermal exchange with the surroundings. The additive effect of the thermo-voltage created by each thermocouple is only possible if their legs are connected as depicted in Fig. 4. The n-type leg has a negative Seebeck coefficient, i.e., the electrons thermally diffuse to the cold side, while in the p-type leg a temperature gradient causes the propagation of holes towards the lower energy region.

3. Thermoelectric Materials

The maximum efficiency of a TEG is governed by material parameters regrouped in the thermoelectric figure of merit Z (see Eq. (9)). Hence, Z can be seen as a measure of a thermoelectric efficiency of a given material. In order to generate an electrical power ($P = VI$, V is the potential, and I the current), a thermoelectric material must: (i) transport the current efficiently, i.e., possess a high electrical conductivity σ; (ii) produce a significant thermo-induced voltage, i.e., be characterized with a high Seebeck coefficient ($V = \alpha\Delta T$) and a low thermal conductivity κ to ensure that a large ΔT is maintained.

Figure 5 displays four classes of materials with respect to the ratio between the electrical and thermal conductivity. Ceramics are heat conductors and electrical insulators ($\sigma < 10^{-7}\,\mathrm{S/cm}$). Amorphous materials such as glasses or plastics are both thermally and electrically insulators ($\kappa < 2\,\mathrm{WK^{-1}m^{-1}}$). Metals or highly doped semiconductors are characterized with high electrical conductivity but high thermal conductivity. Indeed, in electrically conducting materials, heat is transported both through phonons (lattice contribution to the thermal conductivity κ_L) and electrons (electronic contribution κ_e) such that:

$$\kappa = \kappa_e + \kappa_L, \tag{12}$$

$$\kappa_e = LT\sigma. \tag{13}$$

Equation (13) is the Wiedemann–Franz's law that shows the relationship between the electrical conductivity and the electronic contribution to the thermal

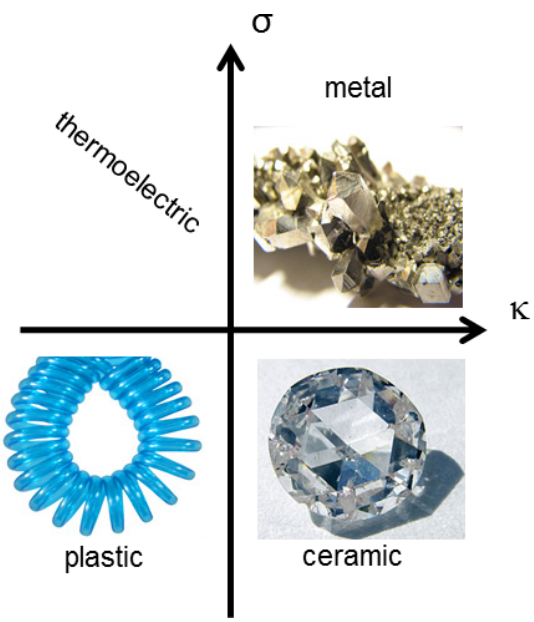

Fig. 5. Different materials classified with respect to their thermal κ and electrical σ conductivities.

conductivity. L is Lorentz factor equals to $2.4 \times 10^{-8}\,J^2K^{-2}C^{-2}$ for a free electron gas. Thermoelectric materials constitute a special class of materials with low thermal conductivity and high electrical conductivity (Fig. 5); often described as "a phonon-glass and electron-crystal" material.[4] Conducting polymers have a low thermal conductivity like amorphous system but they are electrically conducting; thus belonging *a priori* in the family of thermoelectric materials rather than the others.

The best thermoelectric materials possess ZT values around unity. Bismuth chalcogenides are found to be the best materials for room temperature applications with $ZT > 1$.[5] The latter alloys are typically used in radioisotope thermoelectric generators to power satellites. For higher temperatures, inorganic clathrates (e.g., $ZT = 0.87$ at $T = 870\,K$)[6] and Half Heusler alloys (e.g., $ZT = 0.6$ at $T = 800\,K$[7]) have shown assuring thermoelectric efficiency. The study of skutterudite materials (e.g., $ZT = 1.4$ at $T = 900\,K$.[7,8]) that can potentially be extremely efficient is on the way. Promising thermoelectric materials based on atoms of high natural abundance and low toxicity, such as silicides (e.g., $ZT = 0.62$ at 800 K for p-type manganese silicides)[9] and oxides (e.g., $ZT = 0.87$ at 973 K for $(Ca_2CoO_3)_{0.7}CoO_2$),[10] are currently under scientific scrutiny as they are believed to be suitable for the production of TEGs in vehicles, incineration plants, etc.[11] However no efficient thermoelectric materials of high abundance have been found for low temperature applications (<500 K).

4. Doping

Conducting polymers were discovered in the late seventies when it was demonstrated for the first time that poly(acetylene) exposed to iodine vapors could become conductive through a redox reaction.[12–14] As a result, the electrical conductivity increased from 10^{-9} S/cm to 10^5 S/cm followed by a formation of a metal-like low-weight and flexible material, which subsequently became known as a "synthetic metal".[14] Since then, many conjugated polymers characterized by a tunable electrical conductivity have been synthesized. This phenomenon is sometimes called "doping" in analogy with inorganic semiconductors. There are however major differences. For conducting polymers, a counterion not covalently bound to the polymer neutralizes the doping charge carried by the polymer chain. Also, dopant concentrations lie in ppm for inorganics but from few percent up to 35% for conducting polymers. Neutral or undoped conjugated polymers have electrical conductivity values close to insulators, while oxidized or doped conjugated polymers are called conducting polymers because they show similarities with doped semiconductors and sometimes metals. Note that a reduction of a conjugated polymer is also possible, equivalent to an n-doping in inorganic materials, but in this form, many polymers are typically unstable.[15] The search for stable n-type conducting polymers is a timely topic.

There are two possible ways to increase the doping level of a conjugated polymer to make it conducting. In case of electrochemical doping, the conjugated polymer

is in contact with a metal electrode and an electrolyte. The extra charge carriers are provided by the metal electrode. Small counterions, i.e., ions with opposite charge, can penetrate in the polymer to maintain its electro-neutrality. This mass transfer is allowed due to weak van der Waals interactions within the polymer. The oxidation [reduction] of a conjugated molecule takes place at a specific applied electric potential, i.e., when the electrochemical potential of the metal electrons corresponds to the ionization potential [electron affinity] of the conjugated segment in the electrolyte medium. The alternative method is the chemical doping or redox reaction. In that case, the polymer is exposed to a gas or dipped in a solution containing an oxidizing agent (molecule of high electron affinity), also called "dopant", that oxidizes the conjugated polymer. The reduced dopant transforms into a negative counterion, anion, neutralizing the positive charge introduced in the π-electron system of the polymer. Examples of such dopants are iodine I_2 transforming in triiodide I_3^- or a solution of the salt $NO^+PF_6^-$ where the NO gas is released while the PF_6^- anion becomes a counterion in the oxidized polymer. One form of polyaniline, the emeraldine base, is oxidized into the conducting emeraldine salt simply by acid treatment.[16] In this specific case of doping, the protons bound covalently to the nitrogen of polyaniline and its positive charge is transferred to the π-electron system. Finally, conducting polymers can directly be synthesized in their oxidized form by electropolymerization[17] or chemical polymerization.[18] In that case, decreasing the oxidation level (undoping) starting from a highly oxidized polymer can be realized through an electrochemical or chemical reaction, using a reducing agent.

The electrostatic interactions between the dopants and the counterions augment the cohesive energy of conducting polymers as compared to their undoped counterparts. Hence highly doped conducting polymers are typically insoluble. The common strategy for solubility enhancement lays in a dispersion formation via micelle-like particles either with a soluble polymeric counterion (polystyrene sulfonate for poly(3,4-ethylenedioxythiophene), PEDOT-PSS).[18] or using ionic surfactant serving as a counterion (camphorsulfonic acid for polyaniline, Pani-CSA).[19] The presence of specific high boiling point solvents favors a better polymer chains organization and can increase the conductivity by several orders of magnitude.[20,21] This morphology effect is called "secondary" doping to distinguish it from the "primary" effect related to the oxidation (doping) level.

In undoped conjugated polymers, the charge transport is reasonably described by phonon-assisted hopping between energy levels in a Gaussian disorder. When not bounded to a counterion, a charge carrier can hop to a next neutral segment under the influence of the electric field. The intrinsically very low charge carrier density in conjugated polymers ($<10^{20}$ $|e|\mathrm{m}^{-3}$)[22] is accountable for their low electrical conductivity:

$$\sigma = \mu|e|n, \tag{14}$$

where n is the charge carrier density, $|e|$ is the elementary charge, μ is the mobility. To increase the electrical conductivity, doping is required. In the process of doping,

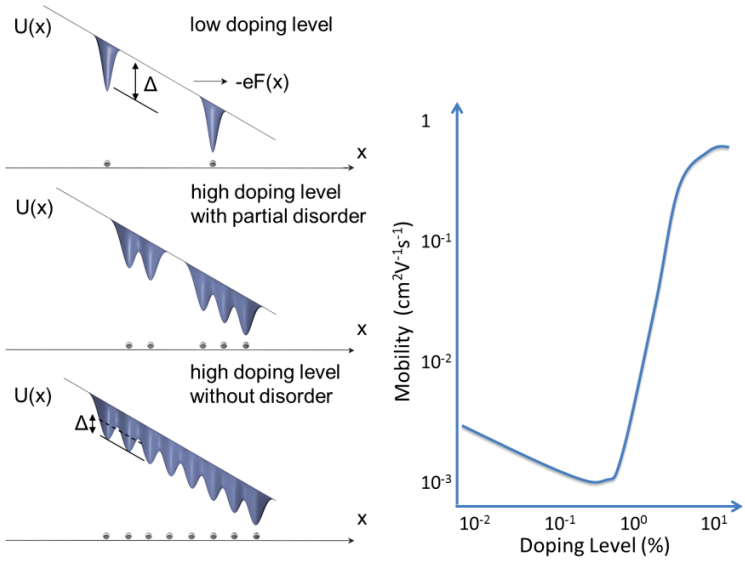

Fig. 6. Electrostatic potential landscape $U(x)$ and reduction of the energy barrier Δ for the charge transport under the influence of an external electric field $F(x)$ created by the counterions for different doping levels and spatial disorder (left) and the effect of doping level on the mobility of charge carriers (right).

extra charge carriers are introduced into the polymer. Once on the chain, they get localized by the traps created by attractive Coulomb potentials of the counterions. Since the dielectric constant of organic materials is very low ($\varepsilon = 3$),[23] the Coulomb traps are rather large in size reaching 20 nm in radius. A single isolated Coulomb trap includes several dozens of hopping sites. Hence, at low doping concentration, the mobility is suppressed by trapping. At higher counterion concentration/doping level (starting from $10^{17}\,\mathrm{cm}^{-3}$) the Coulomb traps begin to overlap and the energy barriers between them tend to decrease (Fig. 6). It translates into energy disorder reduction of the π-orbitals involved in the charge transport and a significant charge mobility increase is expected (e.g., from $10^{-5}\,\mathrm{cm}^2\mathrm{V}^{-1}\mathrm{s}^{-1}$ to $10^{-1}\,\mathrm{cm}^2\mathrm{V}^{-1}\mathrm{s}^{-1}$).[24]

At high oxidation levels (up to 30%) when the distance between counterions is reduced ($\approx$1.5 nm) the electrostatic landscape becomes smooth, i.e., characterized by low energy barriers (Δ) facilitating charge hopping. The electrical conductivity reaches values up to several thousands of S/cm.[25] The positional disorder along with the energetic disorder strongly affects the transport of charge carriers. There are several parameters that govern the positional disorder on the atomic and the microscopic scales such as the position of the counterion, the inter-chain distance, the configuration of the polymer chains, the dimension of crystalline/amorphous domains (defined as the structural coherence length L_{struc}), the orientation of crystalline domains. The wavefunction of the charge carrier tends to be spatially localized by the disorder, this is the so-called Anderson localization.[26] The charge carrier

is characterized by a localization length L_{loc}, which can for instance represent the size of a polaron on one chain or the extension of its wavefunction over stacked adjacent chains. When the crystalline domains are larger than the spatial extent of the carrier ($L_{\text{struc}} > L_{\text{loc}}$), the disorder can be classified as inhomogeneous disorder. Conducting polymers in that situation can be seen as "granular metals" composed of metallic domains surrounded by an amorphous matrix limiting the conductivity.[27,28] The transport mechanism through the amorphous shell is crucial to understanding the transport in macroscopic samples.[29] If $L_{\text{struc}} < L_{\text{loc}}$, the polymer sample has a homogeneous disorder,[30] that is to say, the average electronic coupling or transfer integral between the chains becomes the main parameter governing the interchain transport, and a 3D transport is enabled in a sample comprising aggregated 1D polymer chains.[31,32]

5. Electronic Structure

The conducting polymer chains dissolved in solution show clear modification of their optical properties when their oxidation state is modified.[33] The removal of electrons from the top of the valence band (VB) in a single polymer chain can lead to two different localized positively charged defects: positive polarons (radical cation) and bipolarons (dication) balanced by atomic or molecular counterions. The change in bond length alternation around the excess of positive charge defines the extend of the wavefunction of the (bi)polaron.[34] While the structure of the neutral chain is typically characterized by an aromatic character on cyclic monomers, the polaron distortion appears to have more of a quinoid character, which tends to permute the bond length alternation (double bonds become single bonds and *vice versa*) (Fig. 7).

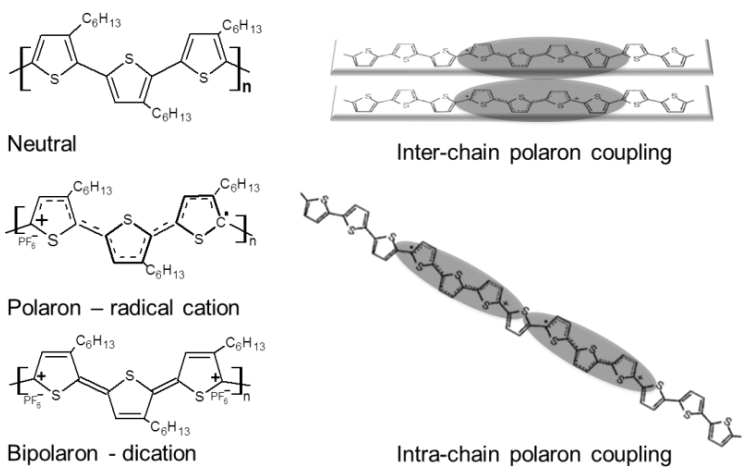

Fig. 7. Chemical structure of a neutral polythiophene chain, as well as a chain that carries a polaron and a bipolaron (left). At high doping level, the coupling between (bi)polarons can be either intra-chain or inter-chain and is at the origin of the creation (bi)polaronic bands (right).

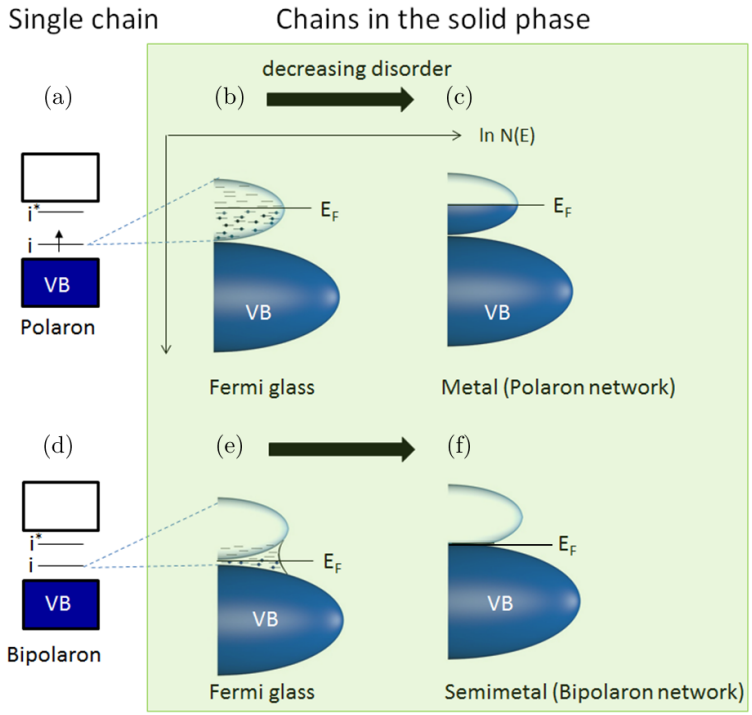

Fig. 8. Electronic structure of a polymer chain with (a) one polaron and (d) one bipolaron on a single polymer chain. Sketch of the logarithm of the density of state ln $N(E)$ for an amorphous (b) polaronic and (e) bipolaronic polymer solid with localized states around the Fermi level E_F; as well as for (c) a metallic network of polarons (metal) and (f) a semi-metallic network of bipolarons with the Fermi level lying in a delocalized band.

This local structural distortion leads to two new in-gap states (i, i*), among which a localized level destabilized from the top of the VB.[34,35] For a polaron, this level "i" is half-filled (Fig. 8(a)); while for a bipolaron, it is empty (Fig. 8(d)). Each of those doping species possesses distinct optical transitions.[33,34] A bipolaron has no spin, whereas a polaron possesses a spin of 1/2 and can be detected by electron spin resonance.[36] Bipolarons are formed rather than two polarons due to subtle energetics involving the Coulomb repulsion between the two charges, the cost in lattice distortion and the electrostatic stabilization due to counterions. The lattice distortion in a bipolaron is more pronounced.[15] than in a polaron with a clear quinoid structure resulting in two empty bipolaronic levels shifted further into the bandgap (Fig. 6).

In the solid state, the polymer chains arrange either in a disorder fashion or self-organize in crystalline domains.[37] In an amorphous phase, polarons or bipolarons levels are localized on a segment of the chains. At high oxidation levels, the wavefunction of the charged defects localized on the same chain overlap and a 1D "intra-chain" band is created.[38] However, this band does not extend through the

three dimension of the solid due to disorder and the absence of the inter-chain electronic coupling.[32] For this reason, in-gap states are spatially localized and spread on an energy distribution. The Fermi level lies among localized states in the middle of the polaron band for a disordered polaronic polymer solid (Fig. 8(b)); or between the VB and the bipolaron band for a disordered bipolaronic polymer solid (Fig. 8(e)).[39] Both solids can be considered as Fermi glasses.[40,41] E_F within localized states implies that the carrier is localized and temperature activated hopping is needed for the transport between localized states. In such situation, $\sigma \to 0$, when $T \to 0$.

In crystalline domains of polymers and in molecular crystals, short inter-chain distances result in an overlap of the π-electronic density of adjacent packed chains; which promotes the delocalization of electronic wavefunction,[42] such as a polaron spreads on several chains (Fig. 7).[43] It is been shown by Mott that for a disordered system the states in the middle of a band are extended states, while those lying in the tails are localized.[44,45] Highly oxidized polyaniline can be a metal[46] characterized with a half-filled polaron band originating from the creation of a polaron network (Fig. 8(c))[47] E_F lies in the region of the extended states, the charge carrier has a large localization length, and the conductivity is metallic: σ increases when cooling down and reaches a finite value at T = 0. When the degree of disorder decreases, polarons form a network and undergo a transition from Fermi glass to metal.[48]

In contrast to polyaniline, polythiophenes like PEDOT are known to facilitate defects like bipolarons.[49] Highly oxidized PEDOT possesses up to one charge carrier per three monomer units.[17] From quantum chemical calculations, a bipolaron in PEDOT spreads over six monomer units or more.[50] In the amorphous bipolaron system (Fig. 8(e)), E_F lays in the localized states fading out from the valence and bipolaron bands. This is also a Fermi glass. For semi-crystalline bipolaronic polymers, a network of bipolaron is formed such that the bipolaron wavefunction overlaps and create an extended empty bipolaron band merging with the filled VB. This is the electronic structure of a semimetal. Like metals, the conductivity diminishes when heating the sample because the delocalized carriers scatter with phonons.

6. Power Factor

As mentioned in the first section, the Seebeck coefficient is intimately related to the electronic structure and mobility of the charge carrier. Mott's formula,[51] which is valid for both hopping and band motion transport mechanisms, states that:

$$\alpha = \frac{d \ln \sigma(E)}{dE} = \frac{1}{\sigma(E)} \frac{d\sigma(E)}{dE}. \tag{15}$$

With Einstein's relation:

$$\sigma(E) = e^2 N(E) D(E), \tag{16}$$

where $D(E)$ is the diffusion coefficient.

$$\frac{d\sigma(E)}{dE} \propto \frac{dN(E)}{dE}\left(D(E) + N(E)\frac{dD(E)}{dN}\right)$$
$$= \frac{dN(E)}{dE}\left(D(E) + N(E)\frac{kT}{e}\frac{d\mu}{dN}\right). \quad (17)$$

since the diffusion coefficient is related to the mobility $\mu = D\frac{e}{kT}$.

For conducting polymers with a high doping level, the mobility is only weakly dependent on the carrier density or doping level (Fig. 6), so that the second term in the last equation can be safely disregarded, i.e., $\mu d/dN \approx 0$. The Seebeck coefficient appears simply related to the slope of the density of states $N(E)$ at the Fermi level.

$$\alpha \propto \left|\frac{dlnN(E)}{dE}\right|_{E_F}. \quad (18)$$

The Seebeck coefficient is small for systems that have a symmetric and slowly varying density of state close to E_F. This is the case of Fermi glasses (Fig. 8(b) and 8(e)) where E_F lays in the localized states fading out from the valence and (bi)polaron bands. It is also the case of metallic polymers since E_F is in the middle of the density of state, thus at its maximum, (Fig. 8(c)). In contrast, conducting polymers composed of a bipolaron network (semimetallic) have an asymmetric $N(E)$ and a large Seebeck coefficient. A first strategy to design a thermoelectric polymer is to choose molecular system where bipolarons are favored (and not polarons) and organize the polymer chains to create a bipolaron network, a semimetallic polymer.

The Fermi glass to semimetal transition is thus characterized by an increase of the Seebeck coefficient α vs. electrical conductivity σ as illustrated in Fig. 9(a).

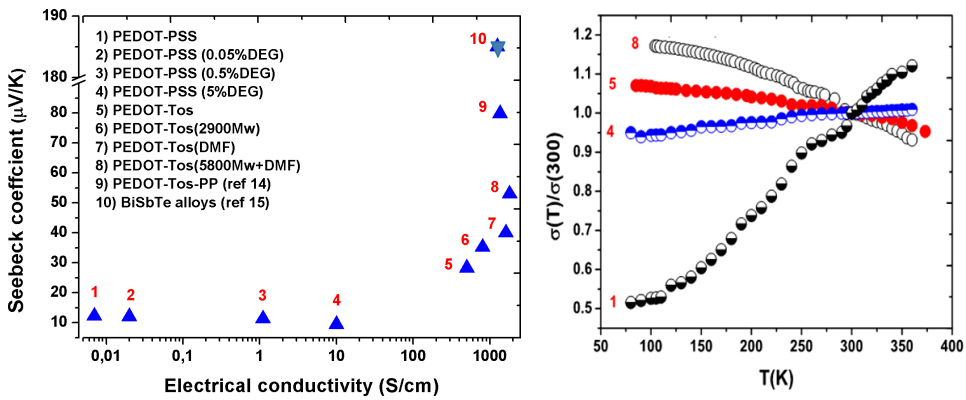

(a) (b)

Fig. 9. (a) (left) Seebeck coefficient vs. electrical conductivity of various PEDOT derivatives. (b) (right) Temperature dependence of the electrical conductivity of few samples corresponding to Fig. 9(a). (reproduced from Ref. [54]).

In that graph, each point correspond to a polymer samples of different degree of crystallinity/molecular organization, amorphous samples have low electrical conductivity and are on the left-hand side. For the sake of comparison, α and σ are also reported for a good thermoelectric material (nanostructured BiSbTe alloy).[52] The Seebeck coefficient and the temperature evolution of the conductivity are clearly correlated. α is almost constant for all polymer samples that shows a temperature activated conductivity (insulator like) (Fig. 9(b)) despite the large variation in σ. α increases drastically for highly conducting samples. When the Seebeck increases, the polymer sample is at the insulator-to-semimetal transition. σ vs. T shows clear negative temperature coefficient at room temperature for the samples with high Seebeck coefficient. The transition from Fermi glass to semimetal is not abrupt indicating that two modes of transport are possibly active simultaneously with different weight: metallic and hopping conductions. It is clear that further improvement in structural order (higher σ) should in principle result in even larger α and thus thermoelectric power factor $\sigma\alpha^2$.

When optimizing inorganic semiconductors for thermoelectric applications, a typical strategy is to tune the doping level to maximize the power factor.[4] Obviously, the increase of charge carrier concentration leads to an enhancement of the electrical conductivity σ and a reduction of the Seebeck coefficient α. Hence, there exists a doping level at which the power factor $\sigma\alpha^2$ is maximum. Similar strategy can be applied to conducting polymers by controlling the doping level. For instance, the oxidation level of the conducting polymer poly3,4-ethylenedioxythiophene-tosylate (PEDOT-Tos) can be decreased by exposure to a chemical reducing agent tetrakis(dimethylamino)ethylene (TDAE).[53] The conductivity experiences a dramatic change as it diminishes from 300 Scm^{-1} at 36% oxidation level down to 10^{-4} Scm^{-1} at 15 % oxidation level (Fig. 10). The Seebeck coefficient α is modified

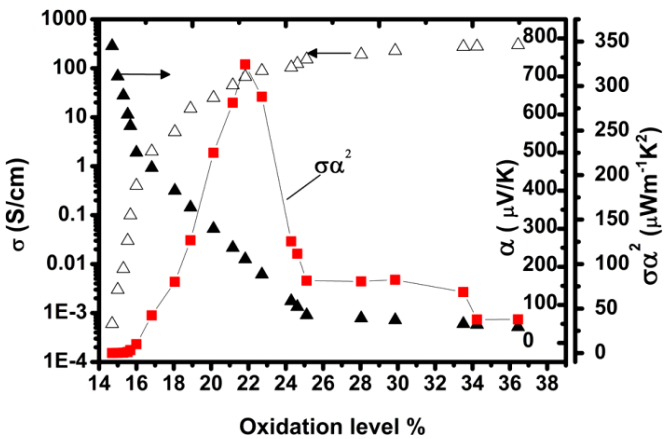

Fig. 10. Seebeck coefficient, electrical conductivity and corresponding power factor $\sigma\alpha^2$ of PEDOT-Tos vs. oxidation level. (Reproduced from Ref. [53]).

by a factor of 20 upon exposing the polymer to the TDAE vapor, such that the power factor $\sigma\alpha^2$ reaches an optimum $324\,\mu\mathrm{Wm}^{-1}\mathrm{K}^2$ at the oxidation level of 22%. At this optimum oxidation level, ZT attains a value of 0.25.

7. Thermal Conductivity

The total thermal conductivity of conducting materials is the sum of an electronic contribution κ_e (charge carriers) and a lattice contribution κ_L (phonons). The electronic contribution to the thermal conductivity of a typical metal can be well described by the Wiedemann–Franz law as $\kappa_e = (k_b/e)^2 L\sigma T$, where k_b is the Boltzmann constant, e is the elemental charge, and L is the dimensionless Lorenz factor, which takes the theoretical Sommerfeld value of $L_0 = \pi^2/3$ for a degenerate Fermi gas such as electrons in a metal. Like for metals, conducting polymers have a non-negligible electronic contribution to the thermal conductivity. Figure 11 displays the total thermal conductivity of thin films of the conducting polymer PEDOT-Tos vs. its electrical conductivity. In these measurements, both heat and electronic currents have the same propagation direction, i.e., along the thin film. In the limit of low electrical conductivity, the thermal conductivity for PEDOT-Tos free standing thin films approaches about $0.5\,\mathrm{Wm}^{-1}\mathrm{K}^{-1}$, which represents an approximation of the lattice contribution, κ_L, to the thermal conductivity. Specifically, the measured thermal conductivity increases with the electrical conductivity, by as much as a factor of three when the electrical conductivity is increased from 20 to about 500 S/cm. Such pronounced increase should not be attributed alone to the variation of κ_L in different samples, and must have an electronic origin. The obtained apparent L is roughly a factor of 2.5 as large as the Sommerfeld value of $L_0 = \pi^2/3$, and shows no clear temperature dependence for PEDOT-Tos.[55] The value of the apparent L depends on the nature of the polymers, and is e.g., close

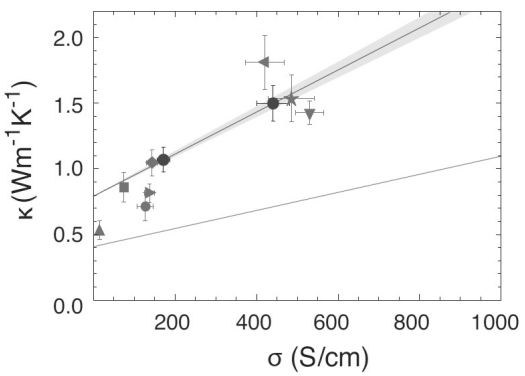

Fig. 11. Thermal conductivity of suspended PEDOT-Tos thin films vs. electrical conductivity at 300K. The top line is a linear fit to the measured data for one sample before and after acid doping, with the range of error in the slope presented as the shaded region. The bottom line indicates the slope given by L_0T. (reproduced from Ref. [55]).

to L_0 for PEDOT:PSS.[56] The origin of the observed deviation in the as-obtained apparent L from the Sommerfeld value is still not clarified.

Regarding the phonon/lattice contribution to the thermal conductivity, no systematic studies have been conducted for conducting polymers with an emphasis on the degrees of crystallinity. However, as far as κ_L is concerned, it is likely that conducting polymers display similar trends as non-conducting polymers. The thermal conductivity of amorphous solid is not well understood and differs very much from that of a crystal. Surprisingly, the thermal conductivity in amorphous solids depends very little on the structure and chemical composition. Notably, for many dissimilar materials such as SiO_2, Se, disorder crystals and polymers the magnitude of thermal conductivities at room temperature is comparable and can be expressed as the minimum thermal conductivity equation[57]:

$$K = \frac{1}{3} C_\nu L, \tag{19}$$

where L is the phonon mean free path, given by the smallest distance in the solid: interatomic distance or interchain distance for polymer, ν is the velocity of sound and C is the classical specific heat. The thermal conductivity of semicrystalline polymers increases with their degree of crystallinity. Also, their thermal conductivity can be anisotropic since polymer chains can be aligned macroscopically due to the fabrication method. For instance, ratio of thermal conductivity measured parallel and perpendicular to a polymer sample $\kappa_{//}/\kappa_{\perp}$ can be as large as 10.[58]

8. Organic TEGs

The main advantages of organic TEGs over inorganic ones are essentially related to inexpensive manufacturing techniques, since conducting polymers can be processed from solution at low temperature. Hence the techniques, such as printing, electropolymerization, drop casting and others are possible. Additionally, polymer-based micro-thermoelectric generators could be fully flexible, which is a key feature for specific applications. Even though the main efforts in the domain of organic thermoelectrics are still aimed at improving further the material's efficiency, the first OTEG prototypes have already been demonstrated.

An early example of a fully organic TEG consisting of 55 legs in a vertical architecture.[53] Each leg is about $1 \times 1.5\,\text{mm}$ of base and $30\,\mu\text{m}$ in length. The legs are obtained by filling cavities with precursor solutions with micropipettes. The cavities are designed with a photoresist on top of the bottom Au electrodes (Fig. 12). The n-legs are composed of a blend of TTF–TCNQ with PVC; while the p-legs are composed of PEDOT-Tos created by direct chemical polymerization of EDOT. The maximum power output was $0.128\,\mu\text{W}$ at $\Delta T = 10\,\text{K}$. The thickness of the device is limiting ΔT, so that higher power could be achieved with longer legs and higher packing density. We therefore extrapolated the expected power generated

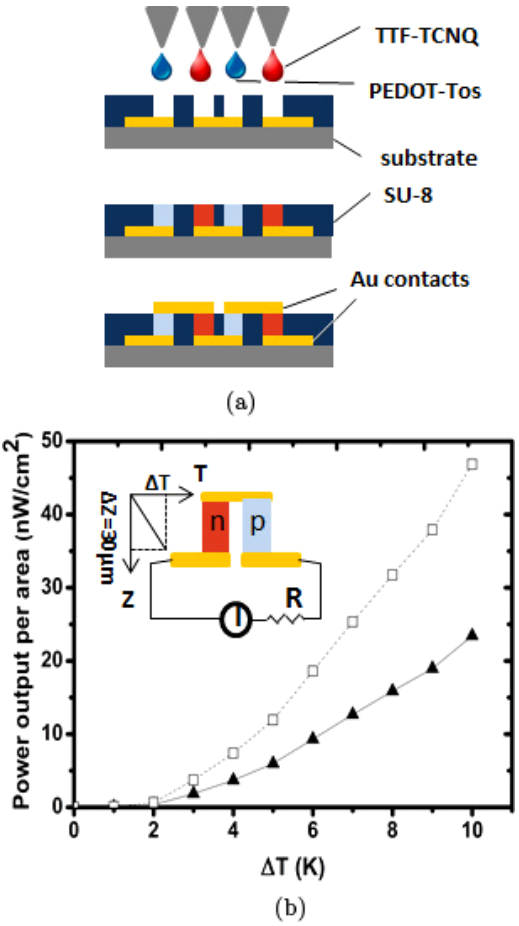

Fig. 12. (a) Thermogenerator fabrication process steps. (b) Maximum power output per area of the PEDOT–Tos/TTF–TCNQ TEGs. The packing density for the matrix, i.e., the area occupied by the legs divided by the total area of the TEG, is 0.47. The extrapolated limit power output for a packing density of 0.94 is plotted in dashed line. (reproduced from Ref. [53]).

per unit area to $0.27\,\mu\mathrm{W\,cm^{-2}}$ at $\Delta T = 30\,\mathrm{K}$. With the manufacturing technique used, this micro-OTEG could easily be composed of many more legs and be flexible.

Already with those early prototypes, OTEGs can potentially drive small electronic devices that usually require not more than 2V. OTEGs can charge supercapacitors able to release a peak power needed for communication technologies. The manufacturing process of miniaturized TEGs fabrication can largely avail of excellent processibility of conducting polymers that can be patterned into thousands of thermocouples scaled down to a small area by printing, drop casting, or electrochemical deposition on rigid or flexible substrates. Furthermore, the restraints imposed on TEGs design are not dictated by the processing limitations but rather by TEGs functionality. These devices can operate at modest temperature gradients

and still exhibit relatively high power generation densities sufficient for applications in autonomous microsystems or wearable electronics. Large area OTEGs for waste heat recovery should consist of multiple OTEG modules delivering reasonable voltage and connected in parallel to supply large current.

9. Conclusion

The optimization of ZT in conducting polymers is only in its infancy and requires a systematic understanding of the influence of morphology, chemical, and electronic structure on three principal thermoelectric parameters. The problem is non-trivial since the thermoelectric properties are related to each other and conducting polymers are known for their morphological complexity and anisotropy of their physical properties. The knowledge available on the structure-charge transport relationship acquired during the last decades on conducting and semiconducting polymers for organic electronics constitutes a strong basis for the development of polymer-based thermoelectrics. A major challenge of this emerging research area is the understanding of the various origins of the Seebeck effect in conducting polymers in order to attain high power factors. Additionally more systematic methods for material thermoelectric properties characterization are required. In order to improve polymer-based organic thermoelectric generators, new manufacturing techniques need to be developed to fabricate micro-TEGs with many hundreds of 10 to 1000 μm-long legs. Today, the perspective of large-scale thermoelectric energy harvesting from waste heat (generated by nuclear reaction or combustion of fossil fuels) and solar heat may seem obscure, but some important efforts are being made to know if this will be possible.

Acknowledgments

The author acknowledges the European Research Council (ERC-starting-grant 307596), the Swedish foundation for strategic research (project: "Nano-material and Scalable TE materials"), the Knut and Alice Wallenberg foundation (project "Power paper"), The Swedish Energy Agency and the Advanced Functional Materials Center at Linköping University. X.C thanks all his coworkers and students for their contributions, discussions and effort during the last years.

References

1. J. P. Heremans, C. M. Thrush, D. T. Morelli and M. C. Wu, Thermoelectric Power of Bismuth Nanocomposites. *Phys. Rev. Lett.* **88**, 216801 (2002).
2. S. O. Kasap, Thermoelectric Effects In Metals: Thermocouples. (2001).
3. R. R. Heikes, R. W. Ure, *Thermoelectricity*: *Science and Engineering* (Interscience, 1961).
4. G. J. Snyder and E. S. Toberer, Complex Thermoelectric Materials. *Nat. Mater.* **7**, 105–114 (2008).

5. W. M. Yim and F. D. Rosi, Compound Tellurides and their Alloys for Peltier Cooling — A review. *Solid State Electron.* **15**, 1121–1140 (1972).
6. V. L. Kuznetsov, A. E. Kaliazin and D. M. Rowe, Preparation and Thermoelectric Properties of A8IIB16IIIB30IV Clathrate Compounds. *J. Appl. Phys.* **87**, 5 (2000).
7. G. J. Poon. In *Semiconductors and Semimetals*, M. Tritt Terry (ed.) (Elsevier, 2001), Vol. 70, pp. 37–75.
8. J.-P. Fleurial, B. A., T. Caillat, D. T. Morelli and G. P. Meisner, In *15th International Conference on Thermoelectrics.* pp. 91–95.
9. W. Luo *et al.* Rapid Synthesis of High Thermoelectric Performance Higher Manganese Silicide with *In-Situ* Formed Nano-Phase of MnSi. *Intermetallics* **19**, 404–408 (2011).
10. M. Shikano and R. Funahashi, Electrical and Thermal Properties of Single-Crystalline (Ca[sub 2]CoO[sub 3])[sub 0.7]CoO[sub 2] with a Ca[sub 3]Co[sub 4]O[sub 9] Structure. *Appl. Phys. Lett.* **82**, 1851–1853 (2003).
11. Y. L. a. R. F. Jian He, Oxide Thermoelectrics: The Challenges, Progress, and Outlook. *J. Mater. Res.* **26**, 10 (2011).
12. A. J. Heeger, Semiconducting and Metallic Polymers:? The Fourth Generation of Polymeric Materials†. *J. Phys. Chem. B* **105**, 8475–8491 (2001).
13. H. Shirakawa, The Discovery of Polyacetylene Film: The Dawning of an Era of Conducting Polymers (Nobel Lecture). *Angew. Chem. Int. Edit.* **40**, 2574–2580 (2001).
14. A. G. MacDiarmid, "Synthetic Metals": A Novel Role for Organic Polymers (Nobel Lecture). *Angew. Chem. Int. Edit.* **40**, 2581–2590 (2001).
15. T. Yamamoto *et al.* pi.-Conjugated Poly(pyridine-2,5-diyl), Poly(2,2′-bipyridine-5,5′-diyl), and Their Alkyl Derivatives. Preparation, Linear Structure, Function as a Ligand to Form Their Transition Metal Complexes, Catalytic Reactions, n-Type Electrically Conducting Properties, Optical Properties, and Alignment on Substrates. *J. Am. Chem. Soc.* **116**, 4832–4845 (1994).
16. J.-C. Chiang and A. G. MacDiarmid, 'Polyaniline': Protonic Acid Doping of the Emeraldine Form to the Metallic Regime. *Synthetic Met.* **13**, 193–205 (1986).
17. G. Zotti *et al.* Electrochemical and XPS Studies toward the Role of Monomeric and Polymeric Sulfonate Counterions in the Synthesis, Composition, and Properties of Poly(3,4-ethylenedioxythiophene). *Macromolecules* **36**, 3337–3344 (2003).
18. L. Groenendaal, F. Jonas, D. Freitag, H. Pielartzik and J. R. Reynolds, Poly(3,4-ethylenedioxythiophene) and its Derivatives: Past, Present, and Future. *Adv. Mater.* **12**, 481–494 (2000).
19. K. Lee *et al.* Metallic Transport in Polyaniline. *Nature* **441**, 65–68 (2006).
20. X. Crispin *et al.* The Origin of the High Conductivity of Poly(3,4-ethylenedioxythiophene)-Poly(styrenesulfonate) (PEDOT-PSS) Plastic Electrodes. *Chem. Mater.* **18**, 4354–4360 (2006).
21. Y. Cao, J. Qiu and P. Smith, Effect of Solvents and Co-Solvents on the Processibility of Polyaniline: I. Solubility and Conductivity Studies. *Synthetic Met.* **69**, 187–190 (1995).
22. C. Tanase, P. W. M. Blom and D. M. de Leeuw, Origin of the Enhanced Space-Charge-Limited Current In Poly(p-phenylene vinylene). *Phys. Rev. B* **70**, 193202 (2004).
23. V. I. Arkhipov, E. V. Emelianova, P. Heremans and H. Bässler, Analytic Model of Carrier Mobility in Doped Disordered Organic Semiconductors. *Phys. Rev. B* **72**, 235202 (2005).
24. G. D. H. Shimotani and Y. Iwasa, Direct Comparison of Field-Effect and Electrochemical Doping in Regioregular Poly(3-hexylthiophene). *Appl. Phys. Lett.* **86**, 3 (2005).
25. Y. Xia, K. Sun and J. Ouyang, Solution-Processed Metallic Conducting Polymer Films as Transparent Electrode of Optoelectronic Devices. *Adv. Mater.* **24**, 2436–2440 (2012).

26. P. W. Anderson, Absence of Diffusion in Certain Random Lattices. *Phys. Rev.* **109**, 1492–1505 (1958).
27. P. Sheng and J. Klafter, Hopping Conductivity in Granular Disordered Systems. *Phys. Rev. B* **27**, 2583–2586 (1983).
28. A. J. Epstein, *et al.* Insulator-to-Metal Transition in Polyaniline: Effect of Protonation In Emeraldine. *Synthetic Met.* **21**, 63–70 (1987).
29. A. B. Kaiser and S. C. Graham, Temperature Dependence of Conductivity in "Metallic" Polyacetylene. *Synthetic Met.* **36**, 367–380 (1990).
30. T. A. Skotheim and J. R. Reynolds, *Handbook of Conducting Polymer.* (Marcel Dekker, 1998), p. 1097.
31. S. Stafström, Conductance and Localization in a System of Coupled Conjugated Polymer Chains. *Phys. Rev. B* **51**, 4137–4142 (1995).
32. V. N. Prigodin and K. B. Efetov, Localization Transition in a Random Network of Metallic Wires: A Model for Highly Conducting Polymers. *Phys. Rev. Lett.* **70**, 2932–2935 (1993).
33. K. Jeuris, L. Groenendaal, H. Verheyen, F. Louwet and F. C. De Schryver, Light Stability of 3,4-ethylenedioxythiophene-based Derivatives. *Synthetic Met.* **132**, 289–295 (2003).
34. J. Cornil, D. Beljonne and J. L. Bredas, Nature of Optical Transitions in Conjugated Oligomers. I. Theoretical Characterization of Neutral and Doped Oligo(phenylenevinylene)s. *J. Chem. Phys.* **103**, 834–841 (1995).
35. J. L. Brédas, F. Wudl and A. J. Heeger, Polarons and Bipolarons in Doped Polythiophene: A Theoretical Investigation. *Solid State Commun.* **63**, 577–580 (1987).
36. F. Devreux, F. Genoud, M. Nechtschein and B. Villeret, Esr Investigation of Polarons and Bipolarons in Conducting Polymers: The Case of Polypyrrole. *Synthetic Met.* **18**, 89–94 (1987).
37. D. C. Martin *et al.* The Morphology of Poly(3,4-ethylenedioxythiophene). *Polym. Rev.* **50**, 340–384 (2010).
38. S. Stafström and J. L. Brédas, Evolution of the Electronic Structure of Polyacetylene and Polythiophene as a Function of Doping Level and Lattice Conformation. *Phys. Rev. B* **38**, 4180–4191 (1988).
39. F. C. Lavarda, M. C. dos Santos, D. S. Galvão and B. Laks, Insulator-to-Metal Transition in Polythiophene. *Phys. Rev. B* **49**, 979–983 (1994).
40. N. S. Sariciftci, A. J. Heeger and Y. Cao, Paramagnetic Susceptibility of Highly Conducting Polyaniline: Disordered Metal with Weak Electron–Electron Interactions (Fermi glass). *Phys. Rev. B* **49**, 5988–5992 (1994).
41. A. J. Heeger, Semiconducting and Metallic Polymers: The Fourth Generation of Polymeric Materials (Nobel Lecture). *Angew. Chem. Int. Edit.* **40**, 2591–2611 (2001).
42. G. Koller *et al.* Intra- and Intermolecular Band Dispersion in an Organic Crystal. *Science* **317**, 351–355 (2007).
43. D. Beljonne *et al.* Optical Signature of Delocalized Polarons in Conjugated Polymers. *Adv. Funct. Mater.* **11**, 229–234 (2001).
44. S. N. F. Mott and E. A. Davis, *Electronic Processes in Non-Crystalline Materials.* (Oxford : Clarendon Press: Oxford University Press, 1979), 2nd edn.
45. G. C. Kopidakis, M. Soukoulis and E. N. Economou, Localization and Electron–Phonon Interactions in Disordered Systems. *Europhys. Lett.* **33**, 459–464 (1996).
46. K. Lee *et al.* Metallic Transport in Polyaniline. *Nature* **441**, 3 (2006).
47. S. Stafström *et al.* Polaron Lattice in Highly Conducting Polyaniline: Theoretical and Optical Studies. *Phys. Rev. Lett.* **59**, 1464–1467 (1987).

48. C. O. Yoon *et al.* Hopping Transport in Doped Conducting Polymers in the Insulating Regime Near the Metal-Insulator Boundary: Polypyrrole, Polyaniline and Polyalkylthiophenes. *Synthetic Met.* **75**, 229–239 (1995).
49. A. Zykwinska, W. Domagala, A. Czardybon, B. Pilawa and M. Lapkowski *In Situ* EPR Spectroelectrochemical Studies of Paramagnetic Centres in Poly(3,4-ethylenedioxythiophene) (PEDOT) and Poly(3,4-butylenedioxythiophene) (PBuDOT) films. *Chem. Phys.* **292**, 31–45 (2003).
50. V. M. Geskin and J.-L. Brédas, Polaron Pair versus Bipolaron on Oligothiophene Chains: A Theoretical Study of the Singlet and Triplet States. *Chem. Phys. Chem.* **4**, 498–505 (2003).
51. M. Cutler and N. F. Mott, Observation of Anderson Localization in an Electron Gas. *Phys. Rev.* **181**, 1336–1340 (1969).
52. Q. H. Bed Poudel, Yi Ma, Yucheng Lan, Austin Minnich, Bo Yu, Xiao Yan, Dezhi Wang, Andrew Muto, Daryoosh Vashaee, Xiaoyuan Chen, Junming Liu, Mildred S. Dresselhaus, Gang Chen, and Zhifeng Ren. High-Thermoelectric Performance of Nanostructured Bismuth Antimony Telluride Bulk Alloys. *Science* **320**, 4 (2008).
53. O. Bubnova *et al.* Optimization of the Thermoelectric Figure of Merit in the Conducting Polymer Poly(3,4-ethylenedioxythiophene). *Nat. Mater.* **10**, 429–433 (2011).
54. O. Bubnova *et al.* Semimetallic Polymers, *Nat. Mater.* **13**, 190–194 (2014).
55. A. Weathers *et al*, Significant Electronic Thermal Transport in the Conducting Polymer Poly(3,4-ethylenedioxythiophene), *Adv. Mater.* **27**, 2101–2106 (2015).
56. J. Liu *et al*, Thermal Conductivity and Elastic Constants of PEDOT:PSS with High Electrical Conductivity, *Macromolecules* **48**, 585–591 (2015).
57. D. G. Cahill and R. O. Pohl, Thermal Conductivity of Amorphous Solids above the Plateau, *Phys. Rev. B* **35**, 4067–4073 (1987).
58. A. G. Gibson, D. Greig, M. Sahota, I. M. Ward and C. L. Choy, Thermal Conductivity of Ultrahigh-Modulus Polyethylene *J. Polym. Sci.* **15**, 183–192 (1977).